Fizika Nizkikh Temperatur, 2007, v. 33, No. 12, p. 1383–1392

From optical spectra to phase diagrams — the binary mixture N_2–CO

M. Vetter[1], A. Brodyanski[1,2], and H.-J. Jodl[1]

[1] *TU Kaiserslautern, Department of Physics, Erwin-Schrödinger-Strasse, Kaiserslautern D-67663, Germany*

[2] *IFOS, Institut für Oberflächen- und Schichtanalytik, TU Kaiserslautern Erwin-Schrödinger-Strasse, Kaiserslautern D-67663, Germany*
E-mail: jodl@physik.uni-kl.de

Received May 30, 2007, revised July 9, 2007

We investigated the *T*–*c*% phase diagram of the binary system N_2–CO. From changes in IR spectra of all kinds of mode excitations (phonons, vibrons) we were able to determine the temperature of phase transitions (solid–solid, solid–liquid). The improvements in comparison to structural investigations by x-rays or electrons are the following: sample growing and handling with perfect optical and thermodynamic quality; determination of actual concentration $(N_2)_x(CO)_y$ from optical spectra; reduction of thermal hysteresis by careful cooling–heating cycles of the samples.

PACS: **78.30.–j** Infrared and Raman spectra;
63.20.Pw Localized modes;
63.20.Ls Phonon interactions with other quasiparticles.

Keywords: phase diagram, IR spectra, optical and thermodynamic quality.

Introduction

All kinds of phase diagrams — such as *T*–*c*%, *V*–*c*%, *p*–*T*, *p*–*V* etc. (*T* — temperature, *c* — concentration, *V* — volume, *p* – pressure) are routinely established on the basis of well tested techniques like x-ray and electron diffraction. The book by Manzhelii [1] contains about 50 phase diagrams of binary solutions of molecular crystals (rare gas solids, H_2, N_2, O_2, CO etc.) found by these techniques.

The aim of our work here is i) to reproduce the one or the other phase diagram, ii) to apply a totally different technique (optical spectroscopy including Raman scattering), iii) to use polycrystalline samples (structural techniques use condensed thin films), iv) to determine directly from spectra the real concentrations.

We have chosen the binary solutions N_2–CO (as an ideal system) because of several reasons: it is perfectly solvable; the *T*–*c*% diagram is pretty simple (Fig. 1); thin film condensation for structural investigations as well as growing of large polycrystals for optical spectroscopy can be achieved; all fundamental modes (phonons, vibrons) are Raman and IR active and their spectra are well understood. These studies at ambient pressure will be the basis for high pressure studies on pure CO and N_2–CO system to establish the *p*–*T*–*c*% phase diagram. Our method — from spectra to phase diagrams — should be applicable to other, more complex systems as well.

The paper is organized such that we will describe in the experimental section the production of samples and the determination of the real concentration. The second section contains several optical spectra; from changes in spectral fingerprints we will deduce a revised, improved phase diagram *T*–*c*%. The third section — discussion —

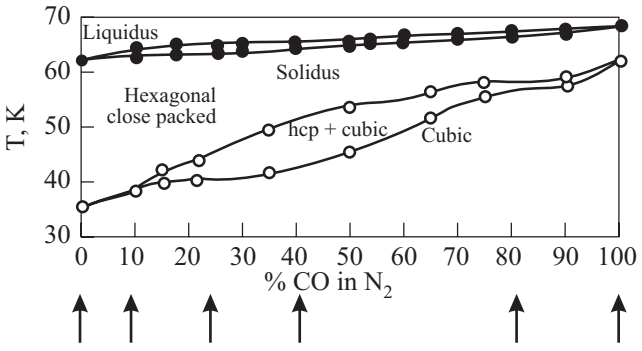

Fig. 1. The N_2–CO phase diagram (taken from [1]), according to calorimetric data (●) from [2] and x-ray diffraction data (○), from [3,4], arrows mark the four mixtures and the pure systems which we studied.

will present interesting questions such as reproducibility of phase transition temperatures, quality of (spectral) data from cooling/heating cycles, thermal hysteresis, accuracy of technical parameters (ΔT, Δc), sample quality in terms of thermodynamic equilibrium, evolution of phase transitions with time.

Experimental

Sample preparation of a mixture with a desired concentration and cooling the sample to an intended p–T point for optical studies is a delicate task (see details [5]). Whereas the same procedure for structural studies is less complicated. To achieve a powder for x-ray or electron diffraction the sample is generally quickly condensated as a thin film. Most of the publications on that matter are not describing experimental details such as cooling rate, if data were found at cooling or heating cycles, amount of time interval to pass a phase transition or to wait till a phase transition is completed etc.

To be successful in growing big polycrystalline samples for optical investigations we followed the general principles of the single crystal growth (see, e.g., Ref. 6) and adapted these for our demands. The sample cell was evacuated up to ~ 10^{-6} mbar at room temperature and purged several times by the investigated gas. After that, the empty cell was cooled down to a temperature that was a bit less than the boiling point of the substance investigated. The sample gas was liquefied at an overpressure of about 0.5 bar. To ensure a complete filling of the sample cell as well as a good thermal contact of our solid sample with walls of the sample cell during crystallization process this gas overpressure was maintained up to finish the crystal growth procedure. In addition this overpressure prevented impurities from outside the system. Changes in our samples during the whole growth procedure were continuously monitored spectroscopically. After condensation, the liquid sample was cooled down (3 K/h) towards the melting point to grow slowly (0.1 K/h) the crystal. At a temperature slightly lower than the crystallization point (ΔT = 0.1–0.5 K), the grown crystal was annealed during 10–20 h. The annealed samples were completely transparent to visible light controlled by eye (microscope) and their continuum transmission was almost equal to that in liquid samples. The averaged cooling rate within the temperature region of high-temperature phases was about 0.5–1 K/h depending on the number of spectra measured in these phases. No significant changes in the continuum transmission of the samples were observed during this time consuming (1–3 days) cooling procedure. In the temperature range of a solid—solid phase transition, the samples were cooled substantially slowly (0.05 K/h). The phase transformation lasted about 2–3 h. Further on, we annealed the crystal of a low-temperature phase during 10–12 h either by keeping the sample at a constant temperature or by very slow (0.02 K/h) cooling. As a result, we obtained big polycrystalline samples of the low-temperature phases of an excellent optical quality.

We measured sample temperature, in the range of 10–80 K, by a calibrated silicon diode, which was directly attached to the sample cell, absolute accuracy of temperature registration was about 0.1 K. This cell with sample chamber (∅ 10 mm; three different thicknesses like 1, 5, and 20 mm) equipped with sapphire windows, was mounted on a cold finger of a closed-cycle He cryostat (see for details [7]). Spectra were recorded in this mid IR region by a Fourier spectrometer (Bruker IFS120 HR) both on cooling and warming cycles. A tungsten lamp was used as the light source, Si on CaF_2 as a beam splitter, and liquid N_2 cooled InSb as the detector (accessible range 1900–11000 cm^{-1}). Our spectral resolution was 0.1–0.5 cm^{-1}, depending on the bandwidth of interest.

There are different ways to determine the real concentration of the actual sample; but we will also briefly describe which errors or awkwardnesses can be made. The wanted concentration c% is produced according to partial pressure of initial gases (N_2 and CO). It takes several days for a uniform gas mixing, depending on the size and form of the gas vessel. During loading the optical cell with the gas mixture and producing the solid sample it depends severely on the p–T conditions during cooling, which real concentration will remain in this sample. Demixing may occur especially in those cases where the gas-liquid transition for both gases is different. In literature about structural studies of binary molecular mixtures we found only statements about concentrations, which were determined from partial pressure. In Raman studies the real concentration is easily found from relative intensities in Raman spectra and known Raman cross sections for vibrations (see Fig. 2 in [8]). In FTIR studies about N_2–O_2 mixtures [9], which are IR inactive, we determined the actual concentration by means of chromatography and mass-spectrometry; after measurements the sample was evaporated into a test volume and was then analyzed. Here we determined the actual concentration via relative intensities I_{pure} and I_{mix} of IR spectra of the (0–2) and (0–3) CO vibration of pure CO in comparison to a mixture of N_2–CO (Fig. 2). The intensity of the vibrations in IR spectra is proportional to the thickness d of the sample, the molar concentration c, and the square of the change in dipole moment. Assuming no significant change of the dipole moment in pure CO and N_2–CO mixtures, the concentration c_{mix} of the mixture is given by

$$c_{\text{mix}} = \frac{d_{\text{pure}}}{d_{\text{mix}}} \frac{I_{\text{mix}}}{I_{\text{pure}}} .$$

The uncertainty in concentration by this method is $\Delta c \approx 5\%$. The impurity concentration of both initial gases

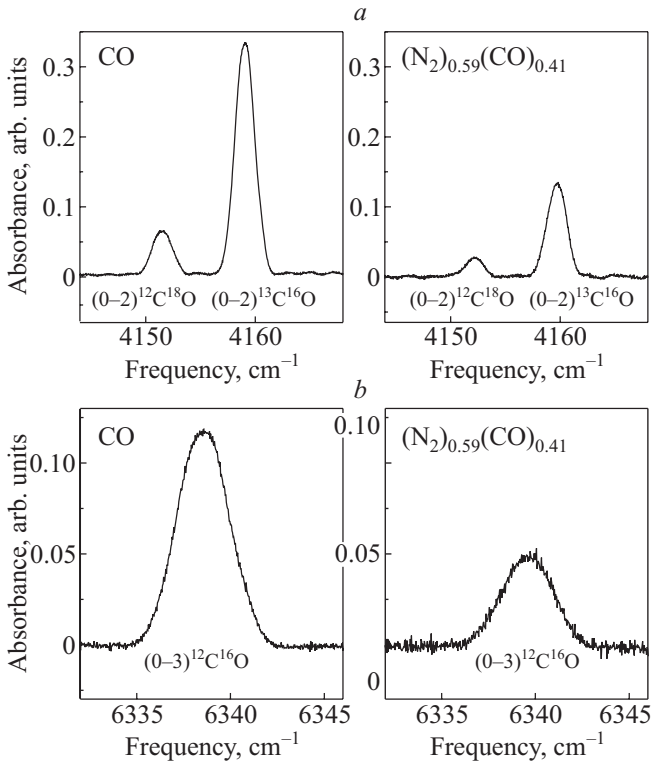

Fig. 2. Method to determine the real concentration *c*%: (0–2) CO mode in pure CO and in a mixture $(N_2)_{0.59}(CO)_{0.41}$ (*a*); (0–3) CO mode in pure CO and in a mixture $(N_2)_{0.59}(CO)_{0.41}$ (*b*).

(N_2, CO) were about < 5 ppm due to information by gas companies.

Results and spectra

In this section we show in detail, how we are able to deduce from characteristics in spectra the position of phase transitions and how we can construct the *T*–*c*% phase diagram. We have chosen several spectral ranges i.e. molecular excitations to demonstrate the power of this method. In detail we will describe only the next one, all the rest will be briefly presented.

Overtone region CO

Figures 3,*a*–*f* are showing IR spectra of the (0–2) CO vibrational mode in pure N_2 (Fig. 3,*a*), in four mixtures (Fig. 3,*b*–*e*) and in pure CO (Fig. 3,*f*); a spectral region around 4250 cm^{-1} (ν_0 = 2139 cm^{-1}). From changes in bandshape we determine the (α–β)-phase transition temperature $T_{\alpha\beta}$. Our pure N_2 gas contains a few ppm CO molecules. In α-N_2 (crystal structure *Pa*3) the (0–2) CO vibrational absorption (around 4253 cm^{-1}) produces a narrow (< 0.1 cm^{-1}) band, whereas in β-N_2 ($P6_3/mmc$ — crystal structure with orientational disorder) this band is very broad (> 5 cm^{-1}). For comparison: the band-

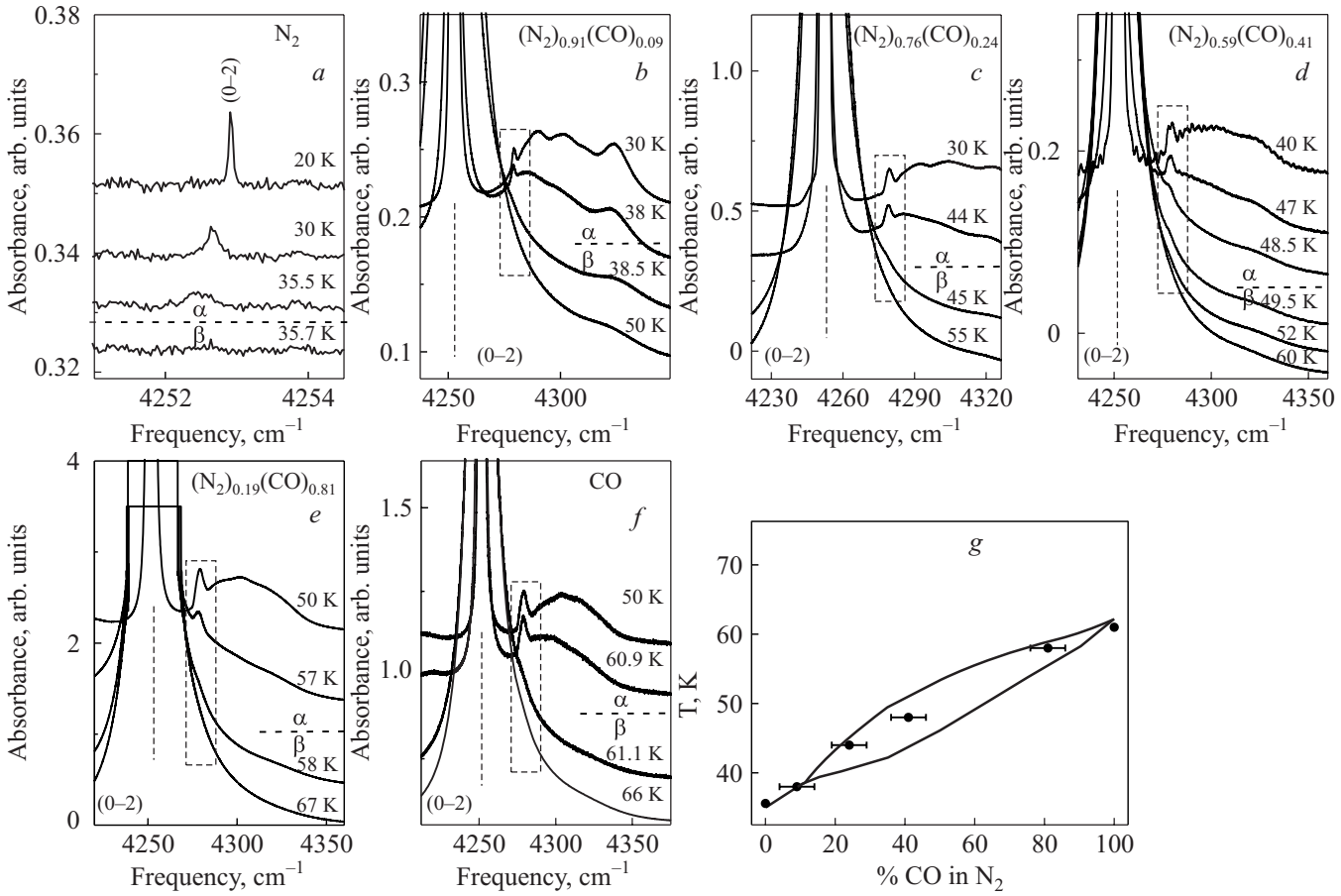

Fig. 3. IR spectra of the overtone region of the CO molecule (around 4250 cm^{-1}) as a function of concentration and temperature, during warming up (*a*–*f*); *T*–*c*% diagram (solid line from Fig. 1) (*g*).

width of the fundamental mode of ppm CO in α-N_2 is ≤ 0.01 cm^{-1} [10]. We find for $T_{\alpha\beta}$ = 35.6 K. The spectrum in pure α–CO (Fig. 3,*f*) contains the very intense (0–2) CO vibron (around 4250 cm^{-1}), the (0–1)(0–1) two vibron band (~ 4280 cm^{-1}) of neighboring CO molecules and a broad phonon sideband to the zero phonon line (ZPL as (0–2) mode). Details and justification for assignment are given in [11]. The (0–1)(0–1) two vibron band, marked by a broken rectangle in Fig. 3,*b–f*, is only IR active in α–CO (crystal structure $P2_13$ with four molecules in unit cell), but IR inactive in β–CO (D^4_{6h} with two molecules in unit cell). We find for $T_{\alpha\beta}$ = 61 K. Similar considerations in IR spectra for the four mixtures are presented in Fig. 3,*b–e*. As a result we are able to construct the *T–c*% diagram (Fig. 3,*g*), which confirms the one from structural analysis (Fig. 1). The main difference is a more narrow region of phase coexistence (hcp + cubic) during cooling/warming cycles, see later.

Second overtone region of CO

Figures 4,*a–e* show IR spectra of the (0–3) CO vibrational model in pure CO and four mixtures (around 6340 cm^{-1}). From distinct changes in bandwidth Γ(*c*,*T*) (Fig. 4,*g*) we determine the (α–β)-phase transition temperature $T_{\alpha\beta}$. The bandwidth is small (~ 1–3 cm^{-1}) in the ordered α-phase and much broader (> 10 cm^{-1}) in the orientational disordered β-phase. Fig. 4,*f* presents the *T–c*% diagram.

Fundamental mode of N_2*:*

Figures 5,*a–c* show the region of the IR nonactive (0–1) vibration of N_2 molecules (~ 2329 cm^{-1}) in three different mixtures N_2–CO. The IR-activity is induced by the presence of neighbouring CO molecules; either by breaking the local translational symmetry and/or by the permanent dipole-moment of CO, which induces a di-

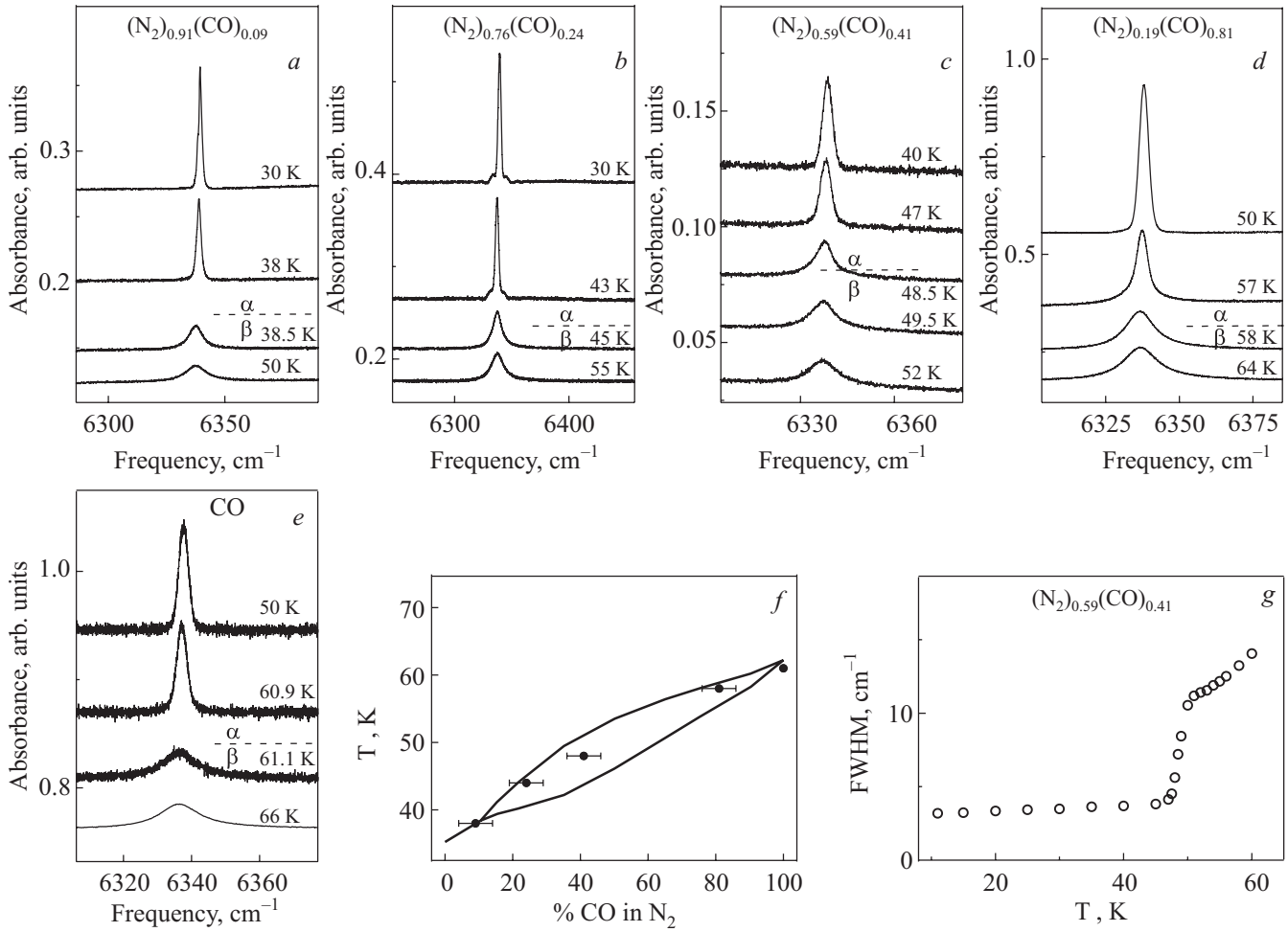

Fig. 4. IR spectra of the second overtone region of the CO molecule (around 6340 cm^{-1}) as a function of concentration and temperature during warming up (the spectrum of concentration $(N_2)_{0.76}(CO)_{0.24}$ (Fig. 4,*b*) at *T* = 30 K shows a «strange» basis at the (0–3) absorption; this is due to the fact that we used only here a thick sample (5 mm); in IR spectra the refractive index must contain real (scattering) and imaginary (absorption) components) (*a–e*); *T–c*% diagram (solid line from Fig. 1) (*f*); Bandwidth Γ as a function of temperature *T* at concentration $(N_2)_{0.59}(CO)_{0.4}$ (*g*).

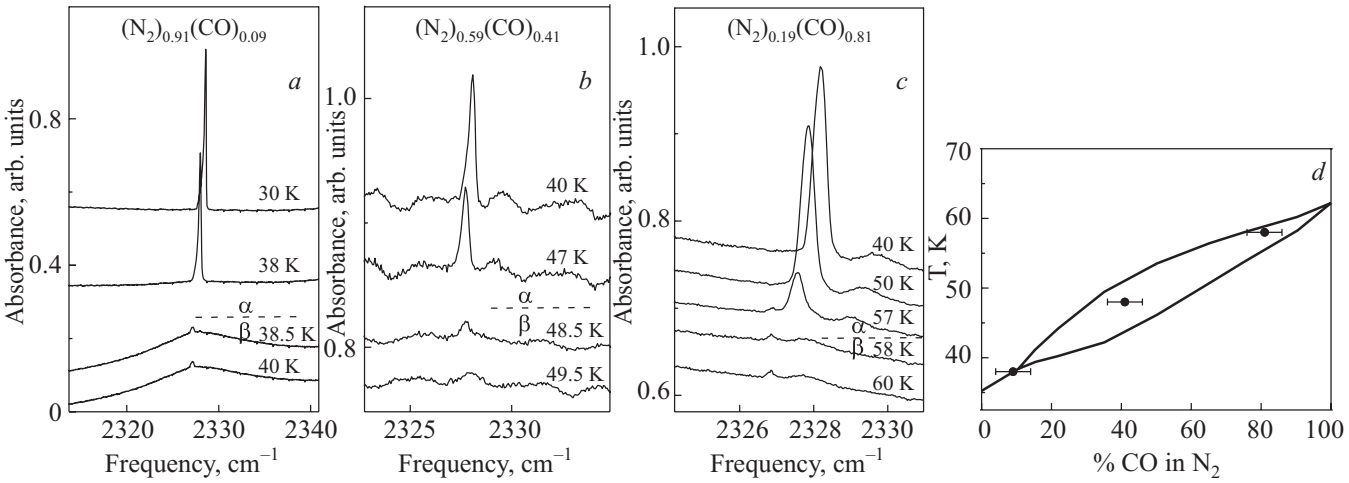

Fig. 5. IR spectra of the N_2 fundamental mode around 2330 cm^{-1} as a function of concentration and temperature; during cooling down (*a*); during warming up (*b,c*); *T*–*c*% diagram (solid line from Fig. 1) (*d*).

pole-moment in N_2 molecules. FTIR spectra of pure optically perfect N_2 crystals contain in that spectral region only a phonon sideband to the fundamental mode of N_2; the shape of the phonon sideband is different in both phases α,β-N_2(Fig. 1 in [5]). The vibron density of states (DOS) is modelled by standard lattice dynamics; only vibron excitations at wave vector $\mathbf{k} = 0$ are known from Raman scattering (see Fig. 22 in [9]). Some details of the shape of the vibron DOS can be deduced from the two-vibron spectra in α-N_2; this is a combinational excitation of (0–1) in one molecule and (0–1) in a neighbouring molecule (Fig. 3 in [11]). With that spectral information and unambiguous assignment we are able now to discuss spectra of Fig. 5. Spectra of the N_2-rich mixture ($(N_2)_{0.91}(CO_{0.09})$) of α*-N_2 (Fig. 5,*a*) are pretty similar to the vibron DOS of the (0–1)(0–1) excitation [12]: broad (~ 1 cm^{-1}), asymmetric triangular band. If we increase concentration of CO this broad asymmetric triangular band is only smeared out. At the (α–β)-phase transition this impurity induced vibron DOS of N_2 disappears in that form. In β-N_2 the N_2-vibration is slightly IR active by the presence of CO molecules and the spectral feature is a broad (~ 30 cm^{-1}) very weak band (Fig. 5,*a*). In a static model we explain the broad band by the absorption of vibrating N_2 molecules, surrounded by and interacting with CO molecules in a partially disordered crystal structure of β*-N_2 i.e. inhomogeniety. In a more dynamic model this broad (~ 30 cm^{-1}) band in the stretching mode region of β-phase is dominated by a quasi-elastic Lorentzian-like component, centered around ν_0 as zero phonon line (ZPL — here ν_0 in N_2 at 2330 cm^{-1}) which we attribute to overdamped orientational modes, i.e. rotational diffusion. The residual feature (a little narrow (< 0.5 cm^{-1}) peak at ν_0 (ZPL) is an IR absorption of a small fraction of N_2 molecules, only vibrating without vibration-rotation coupling. (Similar spectra in Ar:O_2 mixtures, Fig. 2 of Ref. 13.) Fig. 5,*d* shows the found *T*–*c*% diagram.

CO *isotopes*

Figures 6,*a–d* present the region of the (0–2) vibration of several CO isotopes in pure CO and in mixtures (~ 4150 cm^{-1}). The respective fundamental modes (2100–2150 cm^{-1}) generate a very strong absorption in this IR spectra, therefore we studied the overtone region. Since the fundamental frequencies for the isotopes are known and since the natural abundances as well, the spectral assignment is obvious (Table 1).

Table 1. Spectral characteristics of CO isotopes.

CO compounds	Natural abundance [14]	Relative integrated intensity	Frequency of CO in Ne [15], cm^{-1}	Estimated $2\nu_0 - 2\omega_e x_e$ ($\omega_e x_e$ ~ 13 cm^{-1}), cm^{-1}	Our data at 30 K, cm^{-1}
$^{12}C^{16}O$	0.9866 99%	—	~ 2141	4256	4252
$^{13}C^{16}O$	0.0110 1%	5 ~ 100%	~ 2094	4162	4159
$^{12}C^{18}O$	0.0020 0.2%	1 20%	~ 2090	4154	4152
$^{12}C^{17}O$	0.0004 0.04%	0.3 6%	~ 2114	4202	4199

The frequency difference (estimated value — our value, about 2–4 cm^{-1}) is obvious, because the matrix shift in Ne is about 2.4 cm^{-1} and the solid shift is 3.5 cm^{-1} [15].

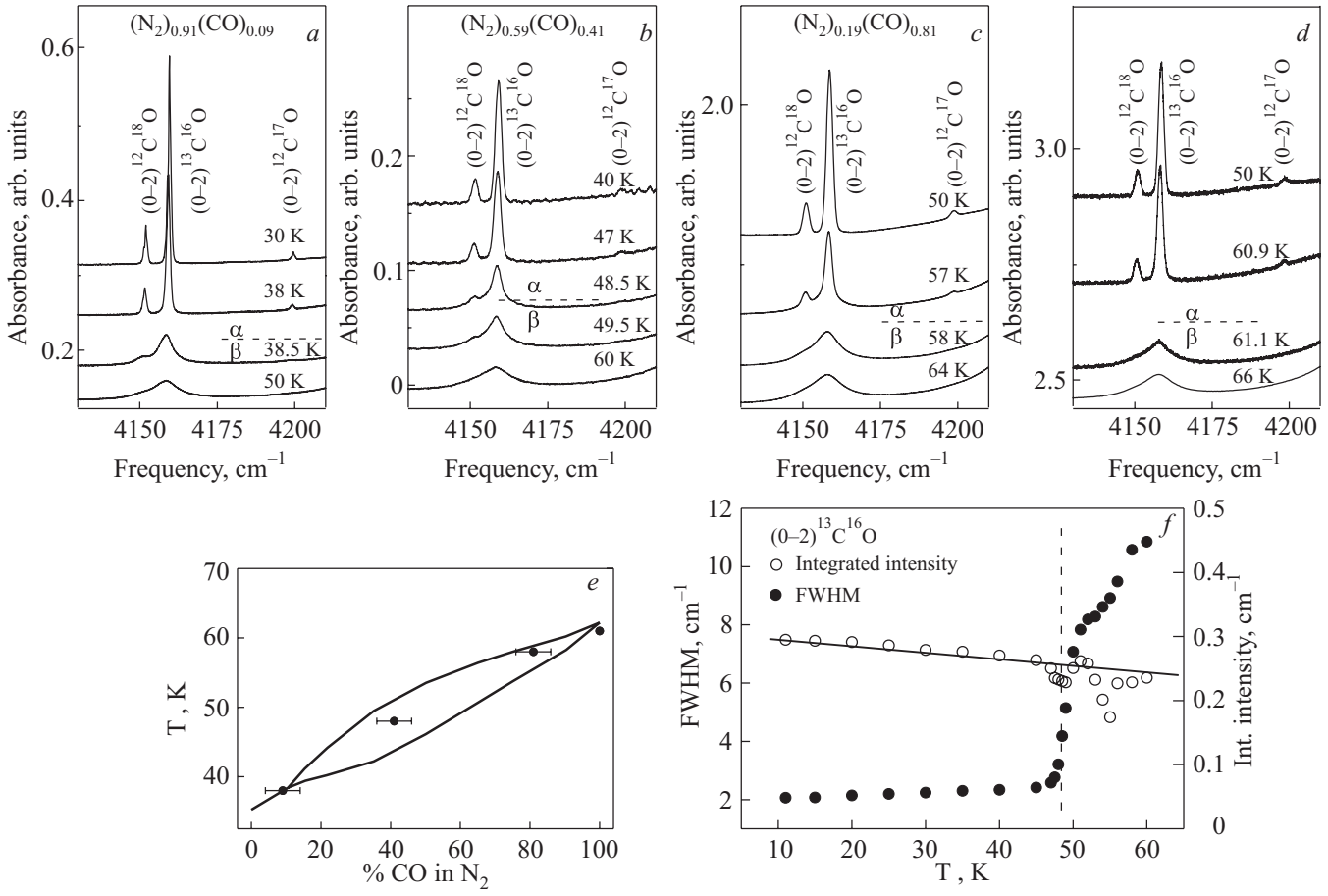

Fig. 6. IR spectra of the overtone region of CO isotopes in pure CO and in mixtures as function of temperature during warming up (*a*–*d*); *T*–*c*% diagram (solid line from Fig. 1) (*e*); evolution of integrated intensity and bandwidth with temperature near phase transition for $(N_2)_{0.59}(CO)_{0.41}$ (*f*).

The isotopes in solid CO or in mixtures represent the matrix-isolated case; therefore we expect a narrow (~ 1 cm^{-1}) band in α-phase and a broad (> 10 cm^{-1}) band in β-phase due to static disorder and/or dynamic interactions. This change in bandwidth at the (α–β)-phase transition is clearly visible in our spectra. Figure 6,*e* shows the found *T*–*c*% diagram. Change in bandwidth Γ(*c*,*T*) and obvious constant integrated intensity *I*(*c*,*T*) are displayed in Fig. 6,*f*.

In general it is difficult to measure integrated intensity with sufficient accuracy (Δ*I* ~ %) and to use this spectral quality for physical arguments. But in our case either optical quality of samples or FTIR-technique were elaborated enough to perform this kind of studies (see Fig. 6,*f* or Fig. 11).

ppm CO_2 *in samples*

Figure 7 shows the region of (0,0,1) fundamental vibration of CO_2 molecules (~ 2348 cm^{-1}) in pure N_2 (Fig. 7,*a*), three mixtures (Fig. 7,*b*–*d*) and in pure CO (Fig. 7,*e*). Similar spectra were also taken of the (0,2,1) mode (~ 3600 cm^{-1}) and (1,0,1) mode (~ 3710 cm^{-1}). From a clear jump in vibrational frequencies at these phase transition we are able to determine the phase transition temperature $T_{\alpha\beta}$. The amount of CO_2 molecules in the initial gas (N_2, CO, or mixtures) is about ppm, due to these gas delivering companies. In a series of papers [7,10] we described in detail this probing technique (*M*/*A* ratio 10^{-6}, *M* — matrix, *A* — impurity; typical *M*/*A* ~ 10^{-3} for standard matrix-isolation technique). In there we explain how we determined the residual amount of CO_2 molecules via optical spectroscopy in combination with other techniques.

The situation of ppm CO_2 in pure N_2 is the easiest case: CO_2 is replaced on one substitutional site in α-N_2 and on two substitutional sites in β-N_2, surrounded by N_2-molecules; this fact gives rise to one or two IR-bands (see for details [10]). The transition temperature is $T_{\alpha,\beta}$ ~ 35.5 K. In pure CO we register in spectra one band due to CO_2 molecules in β-CO and one band in α-CO with a clear frequency jump of this mode (1–2 cm^{-1}) at *T* = 61.0 K (Fig. 7,*g*,*h*). In cooling the α-CO phase this spectrum gets complex and more pronounced. In the three mixtures we find one band of CO_2 molecules

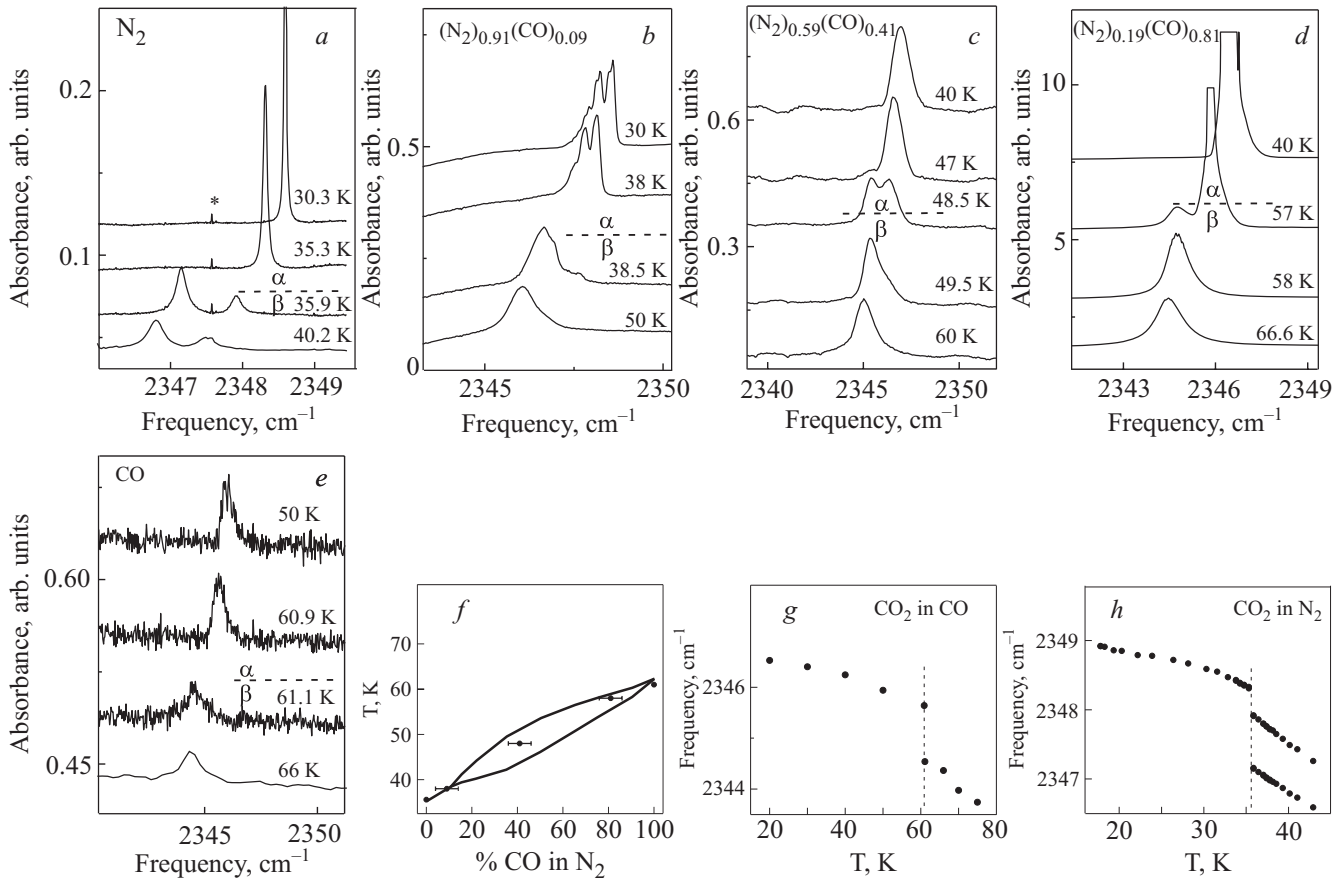

Fig. 7. IR spectra of the fundamental ($\nu_3 \sim 2348$ cm^{-1}) of ppm CO_2 in pure N_2, pure CO and in mixtures as a function of temperatures (*a*–*e*); during cooling down (*a*), during warming up (the peak marked by a star (Fig. 7,*a*) is due to CO_2 molecules condensed externally on the sample cell or as rest gas in the purged sample chamber of the spectrometer) (*b*–*e*); *T*–*c*% diagram (solid line from Fig. 1) (*f*); frequency of this mode as a function of temperature near phase transition in pure CO (*g*) and in pure N_2 (*h*).

in β-CO, one band in α-CO at higher temperatures, with a clear frequency jump of this band at $T_{\alpha\beta}$. In cooling the α-phase of these mixtures we observe a complex and pronounced spectrum (Fig. 7,*b*–*d*); this spectrum looks distinctly different for the N_2 rich case (an asymmetric broad band towards lower frequencies with up to 8 maxima) and for the CO rich case (a broad symmetric band and on top several narrow bands). We interpret these structures in the following way: CO_2 molecule, which is spectroscopically investigated, is surrounded by 12 nearest neighbours, which can be either N_2 or CO molecules due to concentration. In addition the CO molecule has two positions (dipol moment CO, OC; head-tail disorder) [16]. Fig. 7,*f* shows the found *T*–*c*% diagram.

Solid—liquid phase transition

For all three mixtures we have studied the solid-liquid phase transition. We analyzed spectra of three modes, such as a combinational mode around 4460 cm^{-1} ((0–1) vibration of N_2 molecule plus a (0–1) vibration of a neighbouring CO molecule), an overtone mode (0–3) of

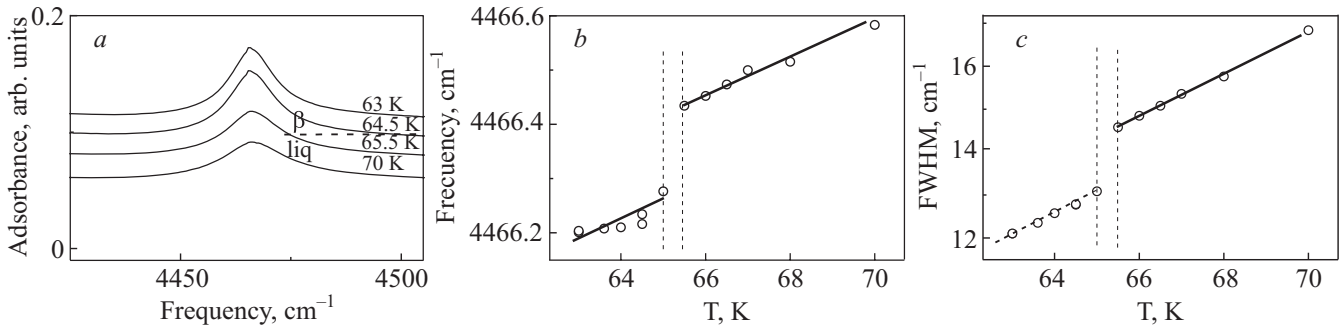

Fig. 8. IR spectra of the combinational mode ((0–1)N_2 + (0–1)CO) of the mixture $(N_2)_{0.59}(CO)_{0.41}$ as a function of temperature during cooling down (*a*); frequency (*b*) and band width (*c*) of this mode as a function of temperature near phase transition.

CO (around 6340 cm^{-1}) and fundamental (0–1) impurity induced N_2 vibration (around 2330 cm^{-1}).

This phase transition is not easy to be monitored spectroscopically. From structural point of view the β-phase (plastic phase i.e. orientational disorder with structural order) is only slightly different from the liquid phase. We studied carefully the (β–ℓ)-N_2 phase transition [5,11]: the volume jump at $T_{\beta\ell}$ is small; dominant short-range orientational order between neighbouring molecules in β and liquid phase play a role. As an example we show in Fig. 8,*a* some spectra of the combinational mode ((0–1)N_2 + (0–1)CO) of the mixture $(N_2)_{0.59}$ $(CO)_{0.41}$ at the (β–ℓ)-phase transition. Looking at spectra only, this phase transition is hardly recognizable; but the detailed analysis, of these spectra reveals this phase transition. Therefore Figs. 8,*b*,*c* displays the change in band frequency ω(*T*,*c*%) and in band width Γ(*T*,*c*%). As a result we find $T_{\beta\ell}$ = 65.5 K; similar results for all 3 mixtures as well as pure cases were found and incorporated, in the *T*–*c*% diagram of Fig. 9.

As a resumee comparing now all results *T*–*c*% from spectra of different mode excitations — such as vibrons, overtone excitations, vibrations, impurity excitations (Fig. 3,*g*, Fig. 4,*e*, Fig. 5,*d*, Fig. 6,*e*, Fig. 7,*f*) — are delivering the same temperature values for the phase transition; i.e. the whole system N_2–CO reacts in the same way, which is a fundamental thermodynamic requirement at a phase transition.

Discussion

In this section we describe a few aspects only such as how reliable our data are, what is the quality of our samples — thermodynamically stable etc.

Phase-diagram

By Fig. 9 we confirm the *T*–*c*% phase diagram of N_2–CO found by other methods (structural and calorimetric analysis) [2–4] and by indirect spectroscopic investigations. The phase coexistence region (hcp and cubic) of low temperature phases is more narrow in our case; as well the solidus—liquid range, i.e. that our method — from changes in optical spectra to phase diagrams — is working and can be applied to the other phase diagrams like pressure/concentration for N_2–O_2 [9] or N_2–CH_4 (in progress); we already finished similar studies at high pressure (p < 10 GPa) and low temperatures (T < 300 K) of pure CO and N_2–CO mixtures [18].

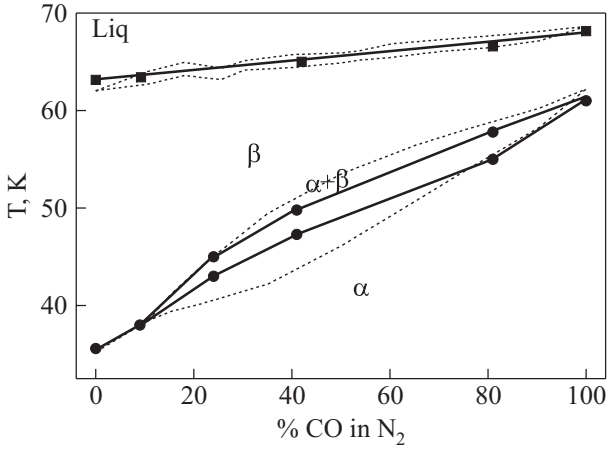

Fig. 9. Refined phase diagram *T*–*c*% of the binary system N_2–CO: our data (●), all the rest from literature, see Fig. 1 (■).

Thermal hysteresis

The reproducibility of our data is well documented in Fig. 10, which is showing spectra of the ν_3-CO_2 mode and ν_0-N_2 in mixture during cooling/heating cycle; even little details of the IR bands are conserved. In general due to experiences with the binary mixture N_2–O_2 [9] we relay more on the second cycle — the warming cycle, because in that case we have thermodynamically stable samples which we proved by spectroscopy (e.g. homogeneous bandwidth); in the first cooling down of the sample overcooling effects may occur which shift phase transitions.

Next we want to answer — via spectroscopy — how broad is the range of phase coexistence hcp/cubic; due to literature about 5–10 K (see Fig. 9). During cooling we

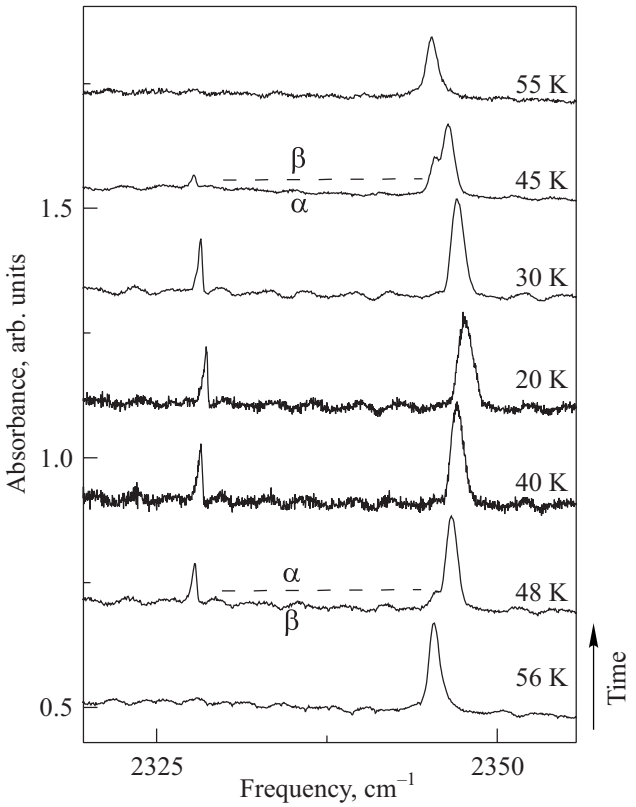

Fig. 10. Reproducibility of spectra: IR spectra of the impurity induced N_2-fundamental mode (around 2328 cm^{-1}) and of the ν_3 mode (around 2345 cm^{-1}) of ppm CO_2 in mixture $(N_2)_{0.59}(CO)_{0.41}$, during cooling and subsequent warming.

determine $T_{\beta\alpha}$, during warming $T_{\alpha\beta}$, do they agree? What is the uncertainty of ΔT for those values. Figures 7,*a–e* are showing the ν_3-mode of ppm CO_2 in pure N_2 (Fig. 7,*a*), in different mixtures (Fig. 7,*b–d*) and in pure CO (Fig. 7,*e*). If we plot for all 5 cases the integrated band intensity of the ν_3-mode of CO_2 as a function of temperature this value must be constant over the whole temperature range; but the same band intensity for this ν_3-mode of CO_2 in one phase is decreasing near phase transition and the band intensity in the other phase must increase accordingly. The range of temperature, where these changes in band intensity are occurring, we define as the range of phase coexistence ΔT. Two examples only: in pure N_2 we find $\Delta T < 0.5$ K (Fig. 11,*a*) and in the mixture $(N_2)_{0.59}(CO)_{0.41}$ we find $\Delta T = 2$ K (Fig. 11,*b*). This range ΔT of phase - coexistence in mixtures should be compared with the thermal hysteresis in pure systems: $T_{\alpha\beta}$(warming) – $T_{\beta\alpha}$(cooling) is about ≤ 0.2 K for pure N_2 and ≤ 0.4 K for pure O_2. This statement is based on IR spectra of ppm CO in these pure systems [7]. Since we used a calibrated Si-diode to measure sample temperature, the uncertainties in temperature is $\Delta T \le 0.1$ K in that range.

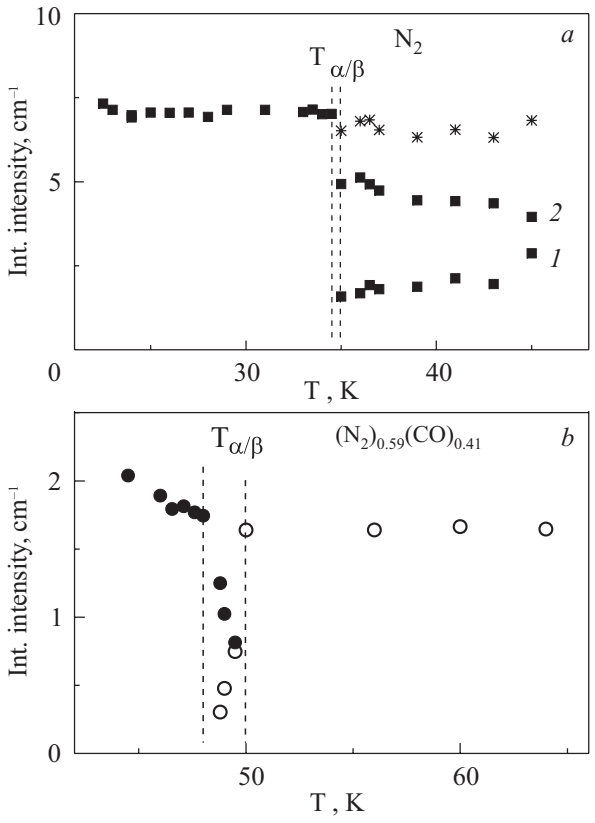

Fig. 11. Phase coexistence region: Integrated band intensity of ν_3-mode of CO_2 in pure N_2 (*a*) and in the mixture $(N_2)_{0.59}(CO)_{0.41}$ (*b*) as a function of temperature are plotted; respective spectra are Figs. 7,*a–c*. In α-phase we observe one band, in β-phase two bands. If we sum the band intensity of band *a* and *b* in β-phase, we get the total band intensity (∗). The range of $\Delta T_{\alpha\beta}$ is marked by vertical lines (*a*). One band in α-phase (●) transforms to one band in β-phase (○); the range of $\Delta T_{\alpha\beta}$ is marked by vertical lines (*b*).

Vibron DOS

The two vibron density of states (DOS) of pure α-N_2 is well measured and modelled by Legay [17]. In addition we studied the temperature evolution of this IR-band around 4650 cm^{-1} ($\nu_0 \sim 2330$ cm^{-1}) (Fig. 3 in [11]).

This combined excitation (0–1)(0–1) between neighbouring molecules requires a perfect crystal from theoretical [17] and experimental [11] point of view. Since N_2 molecules and CO molecules are very similar, especially all their mechanical characteristics (such as mass, moment of inertia, geometrical dimensions) we would expect that the vibron DOS of pure N_2 doped with CO is hardly influenced. Fig. 12 is showing the combined excitation (0–1)(0–1) of N_2 as a function of concentration at lowest temperature.

The spectral feature (width of basis is ~ 1 cm^{-1}) of pure N_2 is like in literature [11]. With increasing amount of CO in this mixture this spectral feature is smeared out (due to CO-impurities), is getting weaker (due to number of N_2-molecules) and is slightly more narrow.

For our kind of studies here the message by Fig. 12 is that all our samples have pretty good crystal quality and

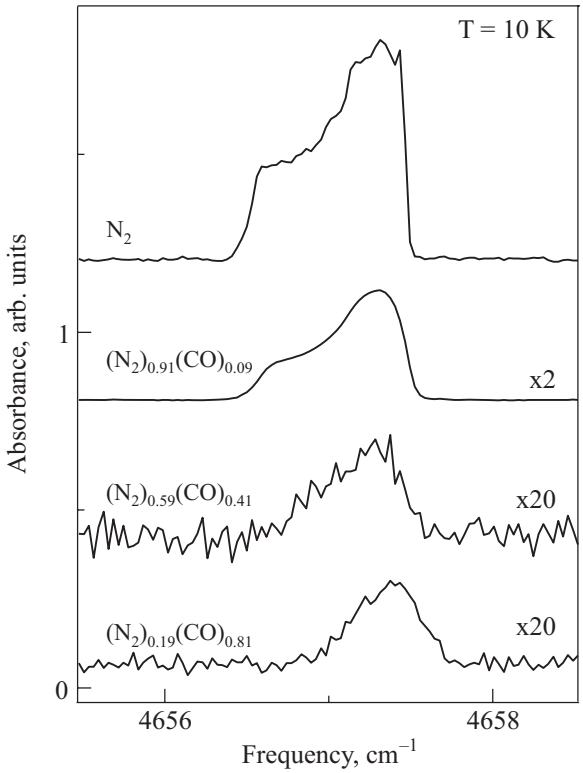

Fig. 12. Vibron DOS: IR spectra of the combined excitation (0–1)(0–1) of neighbouring N_2-molecules at $T = 10$ K in pure N_2 and in mixtures. Increasing the amount of CO in these mixtures, this spectrum of the combined excitation of N_2 is decreasing; therefore we had to multiply these bands with a factor (see right side).

that changes in this vibron DOS of pure α-N_2 by the admixing of CO molecules can be modelled in principle by a theoretical vibron DOS of a mixture and are not simple due to crystal imperfections.

Time dependence of phase transition

We followed the liquid-solid phase transition by visual observation and the (β–α)-phase transition by the changes in the continuum transmission (i.e. changes in the interferogram). As a consequence all phase transitions here in a case of N_2–CO binary mixture used to happen in less than a hour.

Conclusion

We have confirmed the *T*–*c*% phase diagram of the mixture N_2–CO, known by standard structural techniques. From changes in optical spectra of all kinds of mode excitations of these molecules we could clearly determine the temperatures of phase transitions. In addition we succeeded in refining this phase diagram; i.e. a more narrow phase coexistence region hcp/cubic due to better — thermodynamic more stable — crystal quality. As a consequence this method — from optical spectra to phase diagrams — is now applicable to more complicated systems.

This work was supported by the Deutsche Forschungsgemeinschaft (grant No. Jo86-11/2).

1. V.G. Manzhelii, A.I. Prokhvatilov, I.Ya. Minchina, and L.D. Yantsevich, *Handbook of Binary Solutions of Cryocrystals*, Begell House, New York (1996).
2. M. Ruheman, H. Lichter, and P. Komarov, *Phys. Z. Sov.* **8**, 326 (1935).
3. M.J. Angwin and J. Wassermann, *J. Chem. Phys*. **44**, 417 (1966).
4. L. Meyer, *Adv. Chem. Phys*. **16**, 343 (1969).
5. A.P. Brodyanski, S.A. Medvedev, M. Vetter, J. Kreutz, and H.-J. Jodl, *Phys. Rev*. **B66**, 104301 (2002).
6. A.A. Chernov, *Modern Crystallography III: Crystal Growth, Springer Series in Solid-State Sciences*, Springer Verlag, Berlin (1984), v. 336.
7. M. Minenko, M. Vetter, A.P. Brodyanski, and H.-J. Jodl, *Fiz. Nizk. Temp*. **26**, 947 (2000) [*Low Temp. Phys*. **26**, 699 (2000)].
8. M. Minenko, J. Kreutz, Th. Hupprich, and H.-J. Jodl, *J. Phys. Chem*. **B108**, 6429 (2004).
9. M. Minenko and H.-J. Jodl, *Fiz. Nizk. Temp.* **32**, 1382 (2006) [*Low Temp. Phys*. **32**, 1050 (2006)].
10. M. Vetter, M. Jordan, A.P. Brodyanski, and H.-J. Jodl, *J. Phys. Chem.* **A104**, 3698 (2000).
11. M. Vetter, A.P. Brodyanski, S.A. Medvedev, and H.-J. Jodl, *Phys. Rev.* **B75**, 014305 (2007).
12. I.I. Abram, R.M. Hochstrasser, J.E. Kohl, M.G. Semack, and D. White, *J. Chem. Phys.* **71**, 153 (1979).
13. J. Xie, M. Enderle, K. Knorr, and H.-J. Jodl, *Phys. Rev.* **B55**, 8194 (1997).
14. J. Emsley, *The Elements*, Claredon Press, Oxford (1992).
15. H. Dubost, *Chem. Phys*. **12**, 139 (1976).
16. M. Vetter et al., *Head-Tail Disorder in* α-CO *by Matrix-Isolation-Probing Spectroscopy* (In preparation).
17. F. Legay and N. Legay-Sammaire, *Chem. Phys*. **206**, 367 (1996).
18. M. Vetter et al., *Phonon DOS of Phases of Solid* CO *by Optical Studies* (in print).